A Discrete Element approach for Modeling the Thermal-induced Damage in continuous media

G. ALHAJJ HASSAN, W. LECLERC, C. PELEGRIS, M. GUESSASMA, E. BELLENGER

Université de Picardie Jules Verne, MIM, LTI-EA3899, 02100 Saint-Quentin
ghassan.alhajj-hassan@u-picardie.fr

Abstract :

The present paper aims to simulate thermal-induced damage in composite materials using the Discrete Element Method (DEM). We consider a hybrid particulate-lattice model in which discrete elements are linked by cohesive beam elements. First, a model of thermal expansion is introduced at the scale of cohesive link. Second, thermo-elastic behavior of a homogeneous continuous medium is predicted and Discrete Element (DE) results are compared to those obtained by the Finite Element Method (FEM). Then, the case of a unidirectional composite is discussed and some comparisons are done with the FEM in terms of Coefficient of Thermal Expansion (CTE) and stress field. Finally, damage effects and interfacial debonding are taken into account. Results exhibit the ability of the DEM to simulate the suitable damage mode as a function of thermal conditions.

keywords: discrete element method, thermo-elastic behavior, composite, damage effects, interfacial debonding.

1. Introduction

This work is treated in the framework of CUBISM project funded by INTERREG V program. The main objective of the project is to develop a pressure and humidity Surface Acoustic Wave (SAW) sensor in order to follow the drying of refractory materials under high temperature and pressure conditions. More precisely, we aim to describe and predict the thermo-mechanical behavior of the piezoelectric SAW substrate under such conditions for a full set of geometrical configurations and materials. Besides, we expect to take into account the micro-cracks resulting from thermal expansion mismatch between the substrate and its environment. In the present contribution, our main objective is to set up a numerical approach enabling to respond to the above-mentioned issues according to the three following points. First, it has to predict the thermo-mechanical behavior of a given material under potential complex solicitations and severe thermal conditions. Then, the model must take into account the multi-scale features of the material to accurately evaluate the influence of its microstructure on its macroscopic behavior. Finally, the numerical approach has to be flexible enough to simulate several damage modes induced by the thermal expansion mismatch. Please notice that the material substrate has not been defined yet. That is why, we consider in this paper classic materials such as silica and alumina in order to validate the numerical approach. The case of a unidirectional composite material is also envisaged and investigated in this paper.

Several numerical methods have been developed to investigate the failure of materials caused by the crack propagation. The most famous of these methods are based on FEM which uses the principles of fracture mechanics in which the failure condition is defined either by the stress intensity factor or the energy release rate in the specimen. Due to the limitations of FEM to handle fracture mechanic issues accurately, the eXtended Finite Element Method (XFEM) [1] is generally preferred to overcome some difficulties mainly related to mesh updating. However, this method is only well-adapted to describe independent crack propagation without bifurcation and branching but is not suitable for the management of opening and closure of numerous micro-cracks simultaneously.

Another class of methods based on a particulate system also exists. The DEM naturally accounts for discontinuities and is therefore a good alternative to the continuum approaches. The DEM was originally used in the field of rock mechanics [2] and has since widely been developed to become an efficient tool for solving mechanical problems in which multiple scales and discontinuities arise. The discrete approach has also been used in various domains, such as the simulation of tribological granular flow [3], impact effects on concrete [4], vickers indentation [5], silo discharge [6] and frictional multi-contact problems [7]. In addition, the DEM allowed to extract an electrical and measurable response of a bearing in operation [8] and to model heat transfer in continuous medium [9].

Furthermore, several works highlighted the ability of the DEM to simulate the mechanical behavior of continuous materials. In this context, the continuous medium is discretized using a granular packing composed of particles bonded at their contact points using cohesive laws. Two main approaches exist in the literature: the first one is based on the dual spring model (a pair of normal and tangential springs) [10] and the second one lies on the cohesive beam model [11]. Thus, Potyondy and Cundall [12] considered a spring model to simulate a rock material, and Schlangen [11] developed the beam model in 2D to describe the cohesion of the brittle materials. More recently, André et al. [13] considered a hybrid particulate-lattice model using the same paradigm in 3D problems. Moreover, Leclerc et al. [14] discussed a similar model which distinguishes itself by the presence of coupling terms between bending and tangential terms. In other works [15, 16], DEM was later extended to investigate the thermo-elastic behavior of continuous medium using a model of thermal expansion introduced at the scale of cohesive link.

The DEM has also been used to simulate cracks initiation and propagation in homogeneous and composite materials. Researchers have used the discrete approach to study damages of homogeneous materials such as ceramics [17] and also that of heterogeneous materials such as rock [18] and concrete [19]. In such a context, it was proved [20] that the cohesive beam element produces more realistic crack patterns than the spring model. However, one has to keep in mind that the failure model also affects the damage process. Thus, in the case of the beam model, two main microscopic approaches are typically used in the literature : the Removed Discrete Element Failure (RDEF) based on the deletion of a set of particles [21] and the Rankine criterion based on the link failure. In specific cases as the indentation test [21, 22], it was nevertheless verified that the RDEF criterion yields more realistic crack patterns than the bond-based Rankine criterion. Moreover, please notice that some works [16, 23] introduced interfacial debonding in composite material using the Discrete Damage Zone Model (DDZM) [24].

The cohesive beam element approach is based on the discretization of a continuous medium by a granular packing typically composed of spheres in contact, where the cohesion is introduced between each pair of particles in contact using beam elements. In this work, we use granular packings generated by Lubachevsky-Stillinger algorithm [25] which enables an accurate control of intrinsec parameters such

as the compacity, the size of particles and the coordination number which is defined as the average number of contacts per discrete element. Please notice that all our simulations are carried out using parallel MULTICOR3D++ code, in which the hybrid particulate-lattice model discussed by Leclerc [14], is introduced. In this approach and under several assumptions related to the arrangement of particles, the granular packing can be described as an equivalent continuous domain the mechanical properties of which can be related to those of beam elements using a calibration process [14].

The present work is outlined as follows. Section 2 is dedicated to a description of the cohesive beam model. Section 3 describes a model of thermal expansion which is discussed in the context of a homogeneous medium and comparisons are done with the FEM. Then, section 4 is dedicated to an application to the case of a unidirectional composite. Some comparisons are done with FEM in terms of CTE, and stress field. Finally, the thermal-induced damage is observed and discussed in the context of the unidirectional composite.

2. Cohesive beam model

The 3D cohesive beam model (Fig. 1) proposed by Leclerc [14] differs from that developed by André [13] by the presence of coupling terms of tangential and bending terms. In this approach, the cohesive contact is described by a set of geometric and physical parameters related to a beam element, namely the length L_μ, the microscopic Young's modulus E_μ, the microscopic shear modulus G_μ, the cross-section A_μ and the quadratic moment I_μ. The cross-section of the beam element is a disk of radius a_μ which depends on the the radii of both particles i and j in contact R_i and R_j and the dimensionless parameter r_μ as follow:

$$a_\mu = r_\mu \frac{R_i + R_j}{2} \tag{1}$$

The cross-section and the quadratic moment of the beam can also be directly connected to r_μ as follows:

$$A_\mu = \pi \frac{r_\mu^2}{4}(R_i + R_j)^2 \tag{2}$$

$$I_\mu = \pi \frac{r_\mu^4}{64}(R_i + R_j)^4 \tag{3}$$

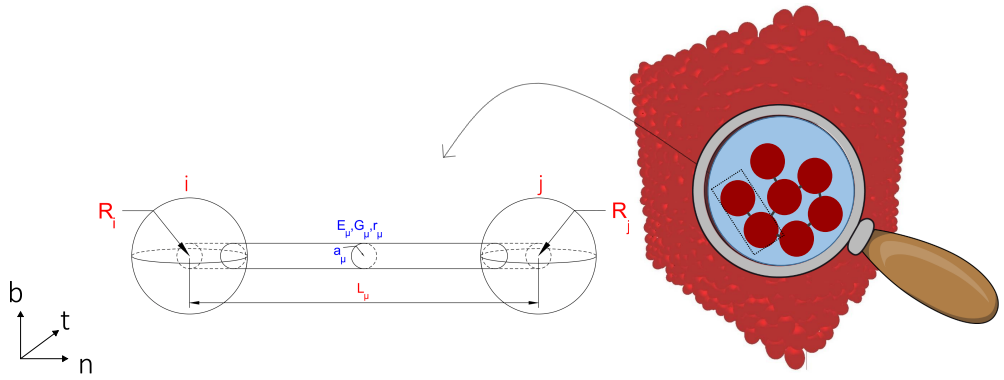

Figure 1: Cohesive beam model

The expression of internal cohesive forces is given by the classical Euler-Bernoulli beam theory [26] in which tensile, bending and torsion effects are taken into account. The following system calculates the interactions between two particles i and j, expressed in the local coordinate system $(\vec{n}, \vec{t}, \vec{b})$ associated to each contact:

$$\begin{bmatrix} F_n^{j\to i} \\ F_t^{j\to i} \\ F_b^{j\to i} \\ M_n^{j\to i} \\ M_t^{j\to i} \\ M_b^{j\to i} \end{bmatrix} = \begin{bmatrix} k_n & 0 & 0 & 0 & 0 & 0 & 0 & 0 \\ 0 & k_t & 0 & 0 & 0 & 0 & \frac{k_t L_\mu}{2} & \frac{k_t L_\mu}{2} \\ 0 & 0 & k_t & 0 & -\frac{k_t L_\mu}{2} & -\frac{k_t L_\mu}{2} & 0 & 0 \\ 0 & 0 & 0 & S_n & 0 & 0 & 0 & 0 \\ 0 & 0 & -\frac{k_t L_\mu}{2} & 0 & \frac{k_t L_\mu^2}{3} & \frac{k_t L_\mu^2}{6} & 0 & 0 \\ 0 & \frac{k_t L_\mu}{2} & 0 & 0 & 0 & 0 & \frac{k_t L_\mu^2}{3} & \frac{k_t L_\mu^2}{6} \end{bmatrix} \begin{bmatrix} u_n^i - u_n^j \\ u_t^i - u_t^j \\ u_b^i - u_b^j \\ \theta_n^i - \theta_n^j \\ \theta_t^i \\ \theta_t^j \\ \theta_b^i \\ \theta_b^j \end{bmatrix}$$

with

- $\vec{n}$ the normal vector aligned with the direction of the beam oriented from i to j, $\vec{t}$ and $\vec{b}$ two tangential vectors on the contact plan,
- $\vec{F}^{j\to i}(F_n, F_t, F_b)$, $\vec{M}^{j\to i}(M_n, M_t, M_b)$ respectively the interaction force and moment applied by the particle j to the particle i, given by their three-components in the local coordinate system ($\vec{n}$, $\vec{t}$, $\vec{b}$),
- $u_n^{i,j}$ and $u_{t,b}^{i,j}$ respectively the normal and tangential displacements associated to the particles i and j,
- $\theta_n^{i,j}$ and $\theta_{t,b}^{i,j}$ the components of rotation respectively in torsion and bending associated to particles i and j,
- k_n, k_t the classical normal and tangential stiffnesses respectively, and S_n a parameter associated to the torsion motion, given by:

$$k_n = \frac{E_\mu A_\mu}{L_\mu} \quad (4) \qquad k_t = \frac{12 E_\mu I_\mu}{L_\mu^3} \quad (5) \qquad S_n = \frac{2 G_\mu I_\mu}{L_\mu} \quad (6)$$

Equations of motion for a given particle derive from internal cohesive forces and the numerical resolution is carried out by an explicit time integration with a formulation based on the Verlet scheme.

The procedure presented by Leclerc [14] enables to identify the macroscopic properties of a sample by realizing a tensile test on a pattern of cubic shape. A calibration process was set up in order to identify the local parameters (E_μ and r_μ) leading to expected macroscopic properties. In addition, based on his work, the minimum number of DE required to represent a continuous homogeneous medium using a representative cubic element is close to 700,000 particles.

3. Thermo-elastic behavior

3.1. Thermal expansion

To describe the thermo-elastic behavior of continuous medium, we introduce a linear thermal expansion coming from literature and recently used by André [15] and Leclerc [16]. In this study, the initial free length of each cohesive link changes according to the temperature. It is extended in the case of an

increase in the temperature of the material and contracted in the case of its decrease (Fig. 2) according to the following equation:

$$l(T) = l^{initial}(1 + \alpha_\mu \, \Delta T) \tag{7}$$

with

- $l^{initial}$ the free length of the cohesive beam at the initial temperature T_0
- $l(T)$ the free length for a given temperature T
- ΔT the temperature variation
- α_μ the CTE associated to the cohesive beam

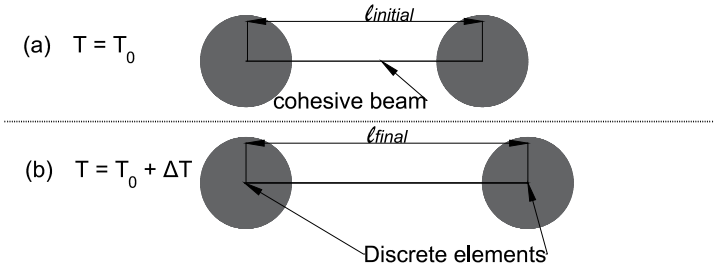

Figure 2: Thermal expansion of the cohesive beam (case of $\Delta T > 0$)

3.2. Homogeneous medium

In the present study, a silica sample of cubic shape composed of 700,000 DE is generated with a macroscopic Young's modulus $E_M = 71$ GPa, a Poisson ratio $\nu_M = 0.15$ and a microscopic CTE $\alpha_\mu = 2.25\ 10^{-5}\ K^{-1}$ associated to cohesive beam. For information, these macroscopic properties correspond to local parameters $E_\mu = 220$ GPa and $r_\mu = 0.722$ and the sample has a cubic shape with length $L = 0.1m$. A variation of temperature (Fig. 3a) is imposed to the homogeneous medium using symmetric boundary conditions.

Then, the macroscopic CTE α_x, α_y and α_z of the pattern are determined in the three directions x, y and z through the displacements of the free faces of the sample. From Figure 3b, two important conclusions can be drawn. First, the macroscopic CTE does not depend on direction, which verifies the isotropy of the system. In addition, the macroscopic CTE converges to that associated to the cohesive contact so that a calibration process for the macroscopic CTE turns out to be useless.

For comparison purposes, a similar study is performed by the FEM, with the same properties of the material, and the same time step $1.3\ 10^{-5}s$. Figures 4a and b show the evolution of the displacement of particles belonging to a free face, and the reaction of the opposite face where symmetry boundary conditions were imposed, as a function of the time, in both approaches. Relative differences between DEM and FEM are less than 5% which could be considered acceptable. We can conclude that this scope of results exhibits a quite good adequation between FEM and DEM.

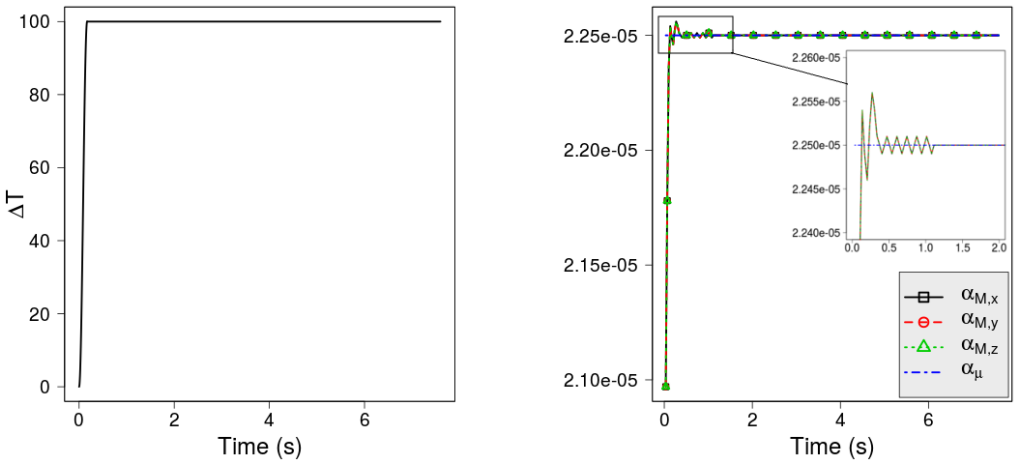

(a) (b)

Figure 3: Evolution of (a) temperature variation (b) macroscopic CTE as a function of the time

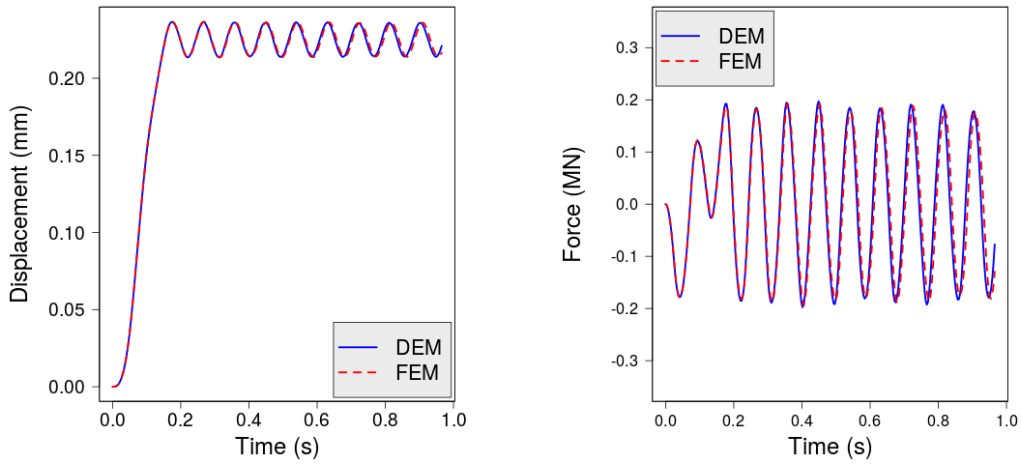

(a) (b)

Figure 4: Evolution of (a) the free edge displacement (b) the force of the opposite face as a function of the time in case of both approaches

4. Case of a heterogeneous medium with a cylindrical inclusion

4.1. Effective CTE

The present section deals with the simulation of a unidirectional composite (Fig. 5) composed of an alumina matrix ($E_m = 350$ GPa, $\nu_m = 0.22$, density $\rho_m = 3900\ kg/m^3$) and a cylindrical metallic inclusion ($E_i = 69$ GPa, $\nu_i = 0.28$, density $\rho_i = 2700\ kg/m^3$). For this purpose, a cubic pattern of length $L = 0.1m$ composed of 2,000,000 DE is used to represent the sample and symmetric boundary conditions are set up. Please notice that the number of DE within the inclusion is close to 390,000 DE which allows to ensure the representativity of the heterogeneous continuous medium [14]. The inclusion is modeled by a cylinder of radius $R = L/4$, so that the theoretical volume fraction is $f_v = 19.6\%$.

For a variation of the contrast c_α between the CTE of the inclusion α_i and the matrix α_m, the effective CTE α_e of the medium is computed using DEM and FEM and compared to Hashin-Shtrikman (HS) analytical approach based on the formulation of Levin [27]. In this study, we distinguish between the axial CTE α_{axial} and the transverse CTE α_{trans}. Figures 6a and b show the effective coefficients for a variation of c_α from $1/100$ to 100. For information purposes, the relative error between the DEM and

the FEM is less than 4%.

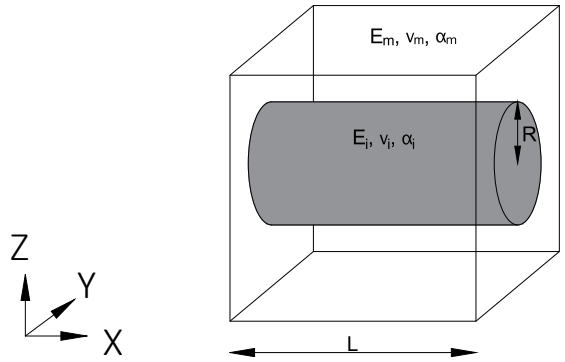

Figure 5: Cubic pattern of the unidirectional composite

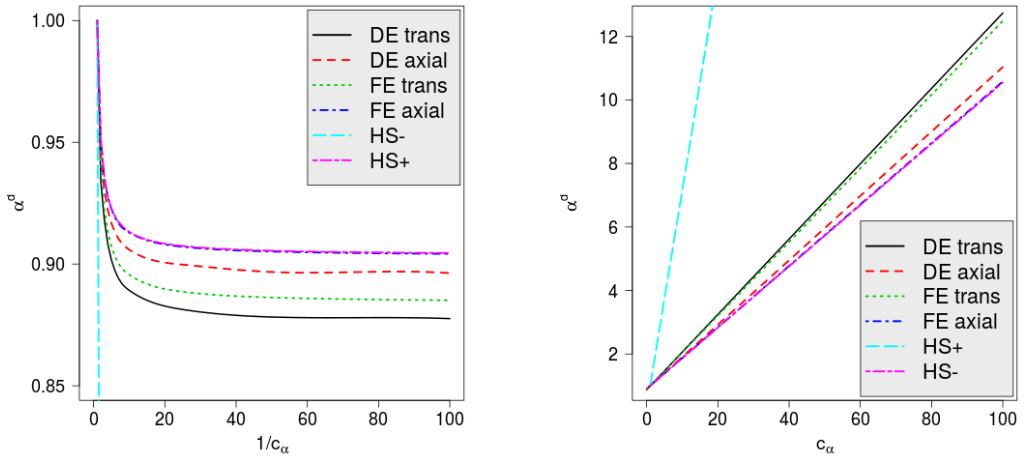

(a) (b)

Figure 6: Evolution of α^d as function of c_α with $\alpha^d = \frac{\alpha_e}{\alpha_m}$ (a) case of $c_\alpha < 1$ (b) case of $c_\alpha > 1$

4.2. Stress field

In this section, we determine the stress field induced by the mismatch of thermal expansion in the case of the unidirectional composite using the DEM. Besides, we aim to highlight certain comparisons with the FEM. Symmetry boundary conditions are imposed in this study and c_α is set to 3 corresponding to the real contrast namely $\alpha_m = 7.5\ 10^{-6}K^{-1}$ and $\alpha_i = 2.25\ 10^{-5}K^{-1}$. Please keep in mind that a representative element is associated to each DE in order to represent the continuum medium. The formulation given by Zhou [28] is used to compute the stress tensor at the scale of a given particle i:

$$\overline{\overline{\sigma}}_i = \frac{1}{2\Omega_i}(\frac{1}{2}\sum_{j\in Z_i} r_{ij} \otimes f_{ij} + f_{ij} \otimes r_{ij}) \tag{8}$$

where $\overline{\overline{\sigma}}_i$ is the equivalent stress tensor associated to particle i, Ω_i is the volume associated to i, f_{ij} is the inter-particle force applied to i by j, r_{ij} is the relative position between i and j and Z_i is the set of particles linked to the particle i. Please notice that Ω_i is computed as follow:

$$\Omega_i = \frac{1}{\phi}V_i \tag{9}$$

with ϕ the volume fraction of DE and V_i the volume of DE i.

Figure 7 illustrates the positive part of the hydrostatic stress in the YZ cutting plane with $X = L/2$ in both approaches for a temperature variation $\Delta T = 10K$. We notice a local variability of the stress field at the scale of particle in DE calculations which is not unexpected since the discrete approach is sensitive to local fluctuations. In order to confront the DEM with the FEM, indicators are introduced at positions A($0.5L$;$0.5L$;$0.875L$), B($0.5L$;$0.5L$;$0.5L$) and C($0.5L$;$0.875L$;$0.875L$) (see Tab. 1). This scope of results exhibits a quite good adequation between FEM and DEM.

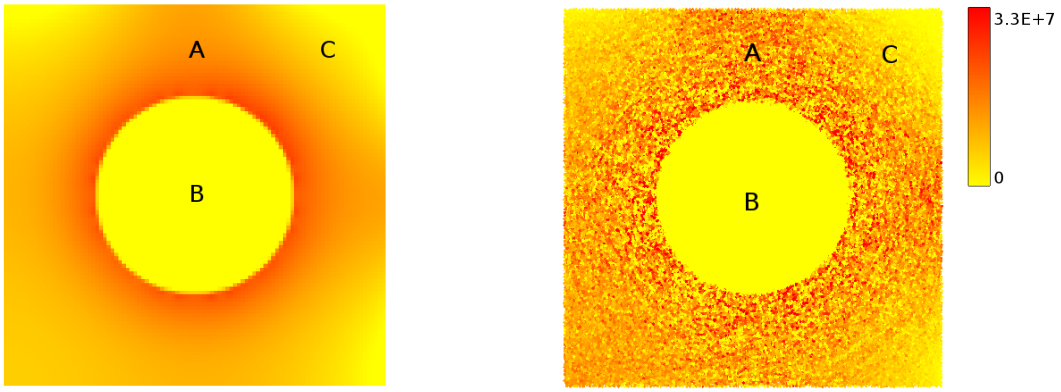

(a) (b)

Figure 7: Hydrostatic stress field (Pa) within the unidirectional composite (a) case of FEM (b) case of the DEM. Extremum values are those predicted by FEM

Table 1: Hydrostatic stress values at A, B and C positions

		position A	position B	position C
σ_{hydro} (MPa)	DE	13.6	-48.4	4.9
	FE	13.6	-45.4	4.7

4.3. Thermal induced damage

We now take into account damage effects and debonding interfacial in the study of the unidirectional composite. In this section, DE calculations are performed using a time step of $4.4\ 10^{-10}s$ and no boundary condition is defined to avoid some boundary effects which could affect the propagation of cracks. We distinguish between two cases, according to the temperature variation. Please notice that the results presented in this section are taken in the YZ cutting plane with $X = 0.5L$.

In the first case, a positive variation of temperature is imposed to the medium with a gradient of $10^{-4}K$ by time step. RDEF criterion [21] is introduced at the scale of particle to simulate cracks propagation of the composite. The RDEF criterion consists in removing the particle and deleting all its links when a given stress based criterion is reached. The removed particles are excluded from the system and no longer act on it, resulting in a loss of mass, but this loss is limited to a low ratio of deleted particles. In this work, we consider the brittle rupture of materials such as alumina and silica. Due to their high compressive strength, the rupture appears when these materials are submitted to tensile solicitations. Therefore, the choice of fracture criterion is based on the hydrostatic stress, at particle scale, which is positive for local tensile solicitations. The hydrostatic stress limit is set to 200 MPa. Figure 8 illustrates

the positive part of the hydrostatic stress field of the composite before and after failure. Cracks start at the interface and propagate within the matrix radially, which is in a good agreement with the theoretical expectations [29].

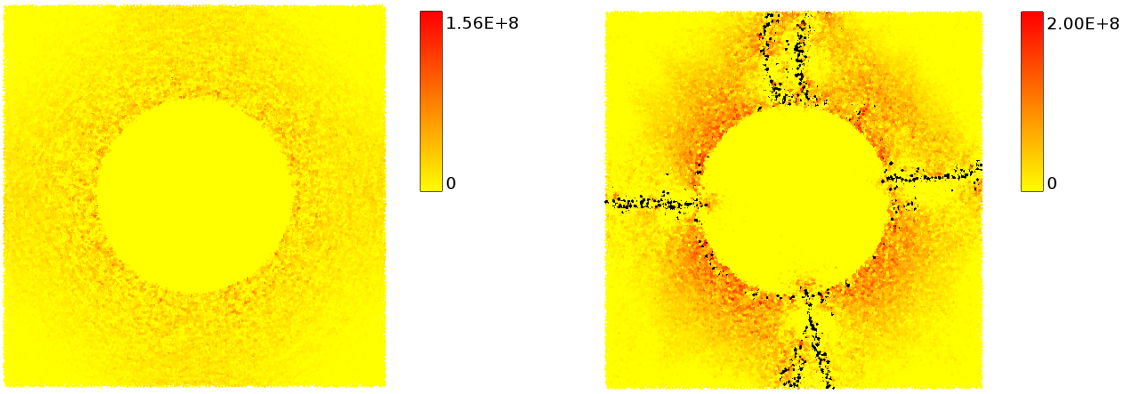

(a) (b)

Figure 8: Hydrostatic stress field (Pa) in case of $\Delta T > 0$ (a) before and (b) after failure (b) The black color corresponds to particles removed from the system

In the second case, a negative variation of temperature is imposed to the composite with a gradient of $10^{-4}K$ by time step. The interfacial debonding could also be the main phenomenon leading to the failure of composite. For that purpose, an interfacial model based on the DDZM [24] is introduced. The main idea is to replace the cohesive links connecting two particles belonging to two different phases by spring elements. The normal stiffness of the spring element K_n^Γ relates the normal displacement u_n^Γ and the normal force F_n^Γ as follows:

$$F_n^\Gamma = K_n^\Gamma u_n^\Gamma \tag{10}$$

In a first linear regime, when $u_n^\Gamma < u_n^{\Gamma,c}$ where $u_n^{\Gamma,c}$ is a critical displacement, K_n^Γ is constant and equal to a given stiffness $K_n^{\Gamma,o}$.

In a second non-linear regime, when $u_n^\Gamma > u_n^{\Gamma,c}$, K_n^Γ depends on u_n^Γ according to an exponential decrease so that K_n^Γ tends to zero for high displacements (see Figure 9). More precisely, in our simulations, the spring element is broken when $u_n^\Gamma > 15u_n^{\Gamma,c}$.

Figures 10a, b, c and d illustrate the positive part of the hydrostatic stress field in the case of $\Delta T < 0$ after 80,000; 170,000; 180,000; and 280,000 time steps. One can notice that the inclusion is totally debonded after 280,000 time steps. From these results, we conclude that the DEM is quite suitable to model the thermal-induced damage in brittle medium.

5. Conclusions and perspectives

This contribution presented a significant improvement for the DEM to model the 3D thermal-induced damage due to thermal expansion. In a first step, a model of thermo-elastic coupling based on a local model of thermal expansion was developed in the case of a homogeneous continuum medium. In a second step, the discrete approach was applied to the context of a unidirectional composite. Some comparisons were done with the FEM in terms of CTE and stress field. In a third step, damage induced by thermal expansion mismatch was modeled. DEM showed its ability to yield a suitable damage mode, namely cracks initiation or interfacial debonding, according to the temperature variation.

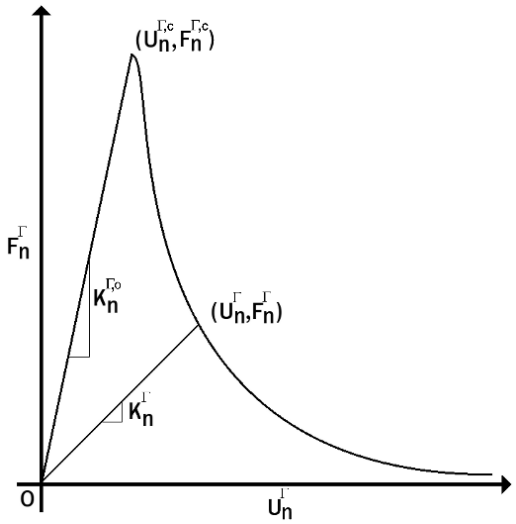

Figure 9: $F_n^{\Gamma} - u_n^{\Gamma}$ relationship

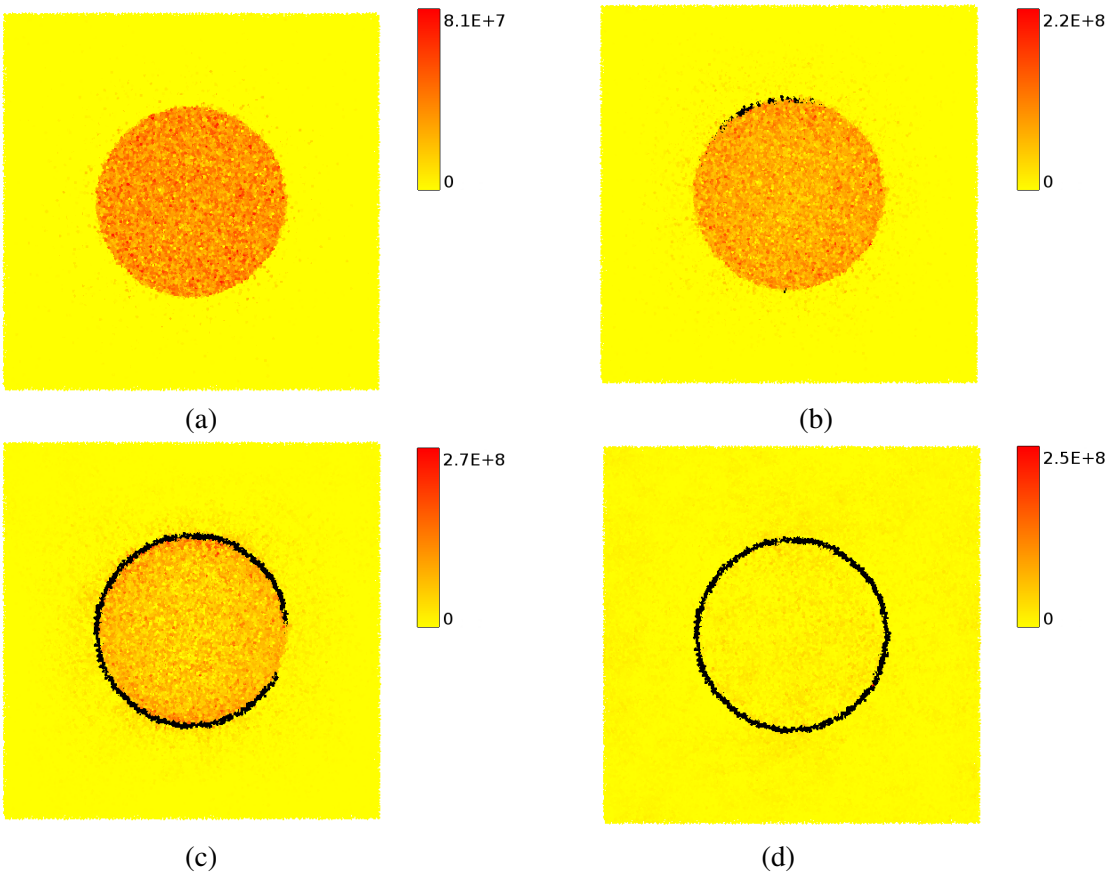

Figure 10: Hydrostatic stress field (Pa) in case of $\Delta T < 0$ (a) after 80,000 time steps (b) after 170,000 time steps (c) after 180,000 time steps (d) after 280,000 time steps
The black color corresponds to spring links broken

In a next future, we aim to develop the present approach to non-linear behaviors. Furthermore, this approach will be extended for modeling the crack propagation in the context of a multi-inclusion composite medium. Besides, we are also interested in better assessing and controlling the local variability observed in stress field at the scale of particle.

References

[1] T. Belytschko and T. Black. Elastic crack growth in finite elements with minimal remeshing. *International Journal for Numerical Methods in Engineering*, 45(5):601–620, 1999.

[2] P. A. Cundall and O. D. L. Strack. A discrete numerical model for granular assemblies. *Géotechnique*, 29(1):47–65, 1979.

[3] N. Fillot, I. Iordanoff, and Y. Berthier. Modelling third body flows with a discrete element method—a tool for understanding wear with adhesive particles. *Tribology International*, 40(6):973 – 981, 2007.

[4] W. Shiu, F.-V. Donzé, and L. Daudeville. Penetration prediction of missiles with different nose shapes by the discrete element numerical approach. *Computers & Structures*, 86(21):2079 – 2086, 2008.

[5] M. Jebahi, D. André, F. Dau, J. l. Charles, and I. Iordanoff. Simulation of vickers indentation of silica glass. *Journal of Non-Crystalline Solids*, 378:15 – 24, 2013.

[6] F. Nicot, N. Hadda, M. Guessasma, J. Fortin, and O. Millet. On the definition of the stress tensor in granular media. *International Journal of Solids and Structures*, 50(14):2508 – 2517, 2013.

[7] I. Sanni, E. Bellenger, J. Fortin, and P. Coorevits. A reliable algorithm to solve 3D frictional multi-contact problems: Application to granular media. *Journal of Computational and Applied Mathematics*, (4):1161 – 1171, 2010.

[8] C. Machado, M. Guessasma, and V. Bourny. Electromechanical prediction of the regime of lubrication in ball bearings using discrete element method. *Tribology International*, 127:69 – 83, 2018.

[9] H. Haddad, M. Guessasma, and J. Fortin. Heat transfer by conduction using dem–fem coupling method. *Computational Materials Science*, 81:339 – 347, 2014.

[10] A. Fakhimi and T. Villegas. Application of dimensional analysis in calibration of a discrete element model for rock deformation and fracture. *Rock Mechanics and Rock Engineering*, 40(2):193, Jun 2006.

[11] E. Schlangen and E.J. Garboczi. New method for simulating fracture using an elastically uniform random geometry lattice. *International Journal of Engineering Science*, 34(10):1131 – 1144, 1996.

[12] D.O. Potyondy and P.A. Cundall. A bonded-particle model for rock. *International Journal of Rock Mechanics and Mining Sciences*, 41(8):1329 – 1364, 2004. Rock Mechanics Results from the Underground Research Laboratory, Canada.

[13] D. André, I. Iordanoff, J. L. Charles, and J. Néauport. Discrete element method to simulate continuous material by using the cohesive beam model. *Computer Methods in Applied Mechanics and Engineering*, 213-216:113 – 125, 2012.

[14] W. Leclerc. Discrete element method to simulate the elastic behavior of 3D heterogeneous continuous media. *International Journal of Solids and Structures*, 121:86 – 102, 2017.

[15] D. André, B. Levraut, N. Tessier-Doyen, and M. Huger. A discrete element thermo-mechanical modelling of diffuse damage induced by thermal expansion mismatch of two-phase materials. *Computer Methods in Applied Mechanics and Engineering*, 318:898 – 916, 2017.

[16] W. Leclerc, H. Haddad, and M. Guessasma. On a discrete element method to simulate thermal-induced damage in 2D composite materials. *Computers & Structures*, 196:277 – 291, 2018.

[17] Y. Tan, D. Yang, and Y. Sheng. Discrete element method modeling of fracture and damage in the machining process of polycrystalline sic. *Journal of the European Ceramic Society*, 29(6):1029 – 1037, 2009.

[18] A. Bobet, A. Fakhimi, S. Johnson, J. Morris, F. Tonon, and M. Ronald Yeung. Numerical models in discontinuous media: Review of advances for rock mechanics applications. *Journal of Geotechnical and Geoenvironmental Engineering*, 135(11):1547–1561, 2009.

[19] S. Hentz, F. V. Donzé, and L. Daudeville. Discrete element modelling of concrete submitted to dynamic loading at high strain rates. *Computers & Structures*, 82(29):2509 – 2524, 2004.

[20] E. Schlangen and E.J. Garboczi. Fracture simulations of concrete using lattice models: Computational aspects. *Engineering Fracture Mechanics*, 57(2):319 – 332, 1997.

[21] D. André, M. Jebahi, I. Iordanoff, J.-L. Charles, and J. Néauport. Using the discrete element method to simulate brittle fracture in the indentation of a silica glass with a blunt indenter. *Computer Methods in Applied Mechanics and Engineering*, 265:136 – 147, 2013.

[22] W. Leclerc, H. Haddad, and M. Guessasma. On the suitability of a discrete element method to simulate cracks initiation and propagation in heterogeneous media. *International Journal of Solids and Structures*, 108:98 – 114, 2017.

[23] B.D. Le, F. Dau, J.L. Charles, and I. Iordanoff. Modeling damages and cracks growth in composite with a 3D discrete element method. *Composites Part B: Engineering*, 91:615 – 630, 2016.

[24] X. Liu, R. Duddu, and H. Waisman. Discrete damage zone model for fracture initiation and propagation. *Engineering Fracture Mechanics*, 92:1 – 18, 2012.

[25] B. D. Lubachevsky and F. H. Stillinger. Geometric properties of random disk packings. *Journal of Statistical Physics*, 60(5):561–583, 1990.

[26] J. S. Przemieniecki. *Theory of Matrix Structural Analysis*. McGraw-Hill, 1968.

[27] V.M. Levin. *On the coefficients of thermal expansion of heterogeneous materials*. Mekhanika Tverdogo Tela 1967.

[28] M. Zhou. A new look at the atomic level virial stress: on continuum-molecular system equivalence. *Proceedings of the Royal Society of London A: Mathematical, Physical and Engineering Sciences*, 459(2037):2347–2392, 2003.

[29] G. Briche, N. Tessier-Doyen, M. Huger, and T. Chotard. Investigation of the damage behaviour of refractory model materials at high temperature by combined pulse echography and acoustic emission techniques. *Journal of the European Ceramic Society*, 28(15):2835 – 2843, 2008.